Modelling of gas conversion with an analytical reactor model for biomass chemical looping combustion (bio-CLC) of solid fuels

N.B. When citing this work, cite the original published paper.

(article starts on next page)

Modelling of gas conversion with an analytical reactor model for biomass chemical looping combustion (bio-CLC) of solid fuels

Daofeng Mei [a,*], Amir H. Soleimanisalim [a], Anders Lyngfelt [a], Henrik Leion [b], Carl Linderholm [a], Tobias Mattisson [a]

[a] Division of Energy Technology, Department of Space, Earth and Environment, Chalmers University of Technology, Gothenburg 41296, Sweden
[b] Department of Chemistry and Chemical Engineering, Chalmers University of Technology, Gothenburg 41293, Sweden

ARTICLE INFO

ABSTRACT

Manganese ores are promising oxygen carriers for chemical looping combustion (CLC), due to their high reactivity with combustible gases. In this work, a manganese ore called EB (Elwaleed B, originating from Egypt) is studied for its reaction rate with CH$_4$, CO and H$_2$ and the data are used in an analytically solved reactor model. The reactivity of fresh and three used EB samples from previous operation in a 10 kW$_{th}$ pilot was examined in a batch fluidized bed reactor with CH$_4$ and syngas (50%CO + 50%H$_2$). In comparison with other manganese ores, the EB ore has a lower rate of reaction with CH$_4$, while showing a significantly higher reactivity with syngas. Nevertheless, this manganese ore always presents a better conversion of CH$_4$ and syngas than the benchmark ilmenite. Mass-based reaction rate constants were obtained using a pseudo first-order reaction mechanism: $1.1 \cdot 10^{-4}$ m^3/(kg·s) for CH$_4$, $6.6 \cdot 10^{-3}$ m^3/(kg·s) for CO and $7.5 \cdot 10^{-3}$ m^3/(kg·s) for H$_2$. These rate constants were used in an analytical reactor model to further investigate results from previous operation in the 10 kW$_{th}$ unit. According to the analytical model, in the 10 kW$_{th}$ operation, 98% of the char in the biomass fuels was gasified before leaving the fuel reactor, while the char gasification products (CO and H$_2$) have a 90% contact efficiency with the bed material. On the contrary, the volatiles have a much lower contact efficiency with the oxygen carrier bed, i.e. 20%, leading to low conversion of volatiles released. Thus, the results emphasize the importance of improving the contact between volatiles and bed material in order to promote combustion performance in the CLC process.

1. Introduction

Thermal energy from combustion provides the major power and energy demand worldwide, while the associated vast amount of emitted CO$_2$ is the main contributor to global warming. Carbon Capture and Storage (CCS) technologies can play an important role in the progress towards a low-carbon future, since neutral and even negative emissions can be realized [1]. As a promising category of CCS technology, Chemical Looping Combustion (CLC) burning fuels without mixing them with air has the advantageous feature of inherent CO$_2$ capture [2–4]. A schematic description of CLC is presented in Fig. 1, showing an air reactor, a fuel reactor and oxygen carrier particles circulating between these reactors. The oxygen carrier is normally metal oxides taking the oxidized form as MeO$_x$ and the reduced form as MeO$_{x-1}$ [5]. In the case of using solid fuels, the fuels are decomposed to char and volatiles upon entering the fuel reactor at a typical temperature of 1073–1273 K, via

pyrolysis reaction (R1). The resultant char is then gasified to CO and H$_2$ by the fluidization steam through reaction (R2). Subsequently, the gasification products (CO and H$_2$) together with volatile combustibles (CH$_4$, CO and H$_2$) react with the oxygen carrier MeO$_x$ via reactions (R3)-(R5), while the oxygen carrier is reduced to MeO$_{x-1}$. After being conveyed to the air reactor, the reduced oxygen carrier is oxidized back to MeO$_x$ by the oxygen in air through reaction (R6). As can be seen in reactions (R3)-(R5), gases from the fuel reactor are mainly CO$_2$ and H$_2$O, where the former can be easily captured after simple steam condensation. When using biomass fuels in CLC, i.e. bio-CLC, the captured and stored CO$_2$ will result in a net-flow of carbon out of the atmosphere, thus achieving negative CO$_2$ emissions [3,6]. The heat released from the CLC process is identical to that of conventional combustion, and can be used for power or heat generation [7–10]. Therefore, CLC is an innovative combustion technology for power and thermal energy generation with low energy penalty and inherent CO$_2$ capture.

---

* Corresponding author.
E-mail address: daofeng.mei@chalmers.se (D. Mei).

Nomenclatures

a	ratio between oxygen demand for CH_4 in volatiles and the total oxygen demand for volatiles
A_c	inner cross-section area of the reactor tube for modelling, m^2
b	ratio between oxygen demand for CO in volatiles and the total oxygen demand for volatiles
bio-CLC	biomass Chemical Looping Combustion
c	ratio between oxygen demand for H_2 in volatiles and the total oxygen demand for volatiles
$C_{i,g}$	concentration of gas i (i = CO or H_2) in the gasification products in the reactor for modelling, mol/m^3
$C_{i,m}$	concentration of component i (i = CH_4, CO or H_2) at coordinate m of the reactor for modelling, mol/m^3
CCS	Carbon Capture and Storage
CFD	Computational Fluid Dynamics
CI	circulation index of oxygen carrier particles between air reactor and fuel reactor, $Pa·m^3/s$
CI_0	base value for circulation index CI, $Pa·m^3/s$
CLC	Chemical Looping Combustion
CLOU	Chemical Looping with Oxygen Uncoupling
g	acceleration of gravity, m/s^2
$k_{F,i}$	mass-based reaction rate constant for gas i (i = CH_4, CO or H_2) and oxygen carrier, $m^3/(kg·s)$
m	coordinate based on oxygen carrier bed mass in the reactor for modelling, kg
m_{ox}	mass of oxygen carrier used in the batch reactor, kg
m_{tot}	total mass of oxygen carrier bed in the reactor for modelling, kg
M_O	molar weight of atomic oxygen, kg/mol
MeO_x	oxygen carrier in the oxidized form
MeO_{x-1}	oxygen carrier in the reduced form
n	molar flow rate, mol/s
n_{CI}	exponential factor considering the effect of circulation index CI on the modelling for overall gas conversion
$n_{i,g}$	molar flow of gas i (i = CO or H_2) from char gasification in the reactor for modelling, mol/s
$n_{i,r}$	consumption rate of gas i (i = CH_4, CO or H_2) via gas-oxygen carrier reactions in the reactor for modelling, mol/s
$\dot{n}_{out}$	total dry gas molar flow after the batch fluidized bed reactor, mol/s
n_T	exponential factor considering the effect of temperature T on the modelling for overall gas conversion
p	partial pressure, bar
p_i	partial pressure of gas i (i = CH_4, CO or H_2), bar
$p_{i,0}$	partial pressure of component i (i = CH_4, CO or H_2) in the

	gas stream entering the reactor, bar
$p_{i,g}$	partial pressure of gas component i (i = CO or H_2) from char gasification in the reactor, bar
R	universal gas constant, $(bar·m^3)/(mol·K)$
t	instantaneous time, s
t_0	time for the beginning of reaction in the batch reactor, s
T	Kelvin temperature, K
T_0	base value for temperature T, K
V	volumetric flow, m^3/s
V_0	total volumetric flow of gas entering the reactor for modelling, m^3/s
V_{CH4}	volumetric flow of CH_4 used for batch-reactor tests with methane, m^3/s
V_g	volumetric flow of gas from char gasification at the bed surface of the reactor for modelling, m^3/s
V_m	total volumetric flow of gas at coordinate m of the reactor for modelling, m^3/s
V_{syn}	volumetric flow of syngas used for batch-reactor tests, m^3/s
x_i	fraction of gas i (i = CH_4, CO_2, CO or H_2) measured by the gas analyzer
α_i	dimensionless number
γ_c	gas conversion for char
$\gamma_{c,i}$	conversion of gas i (i = CO or H_2) from char gasification
$\gamma_{CH4,CH4}$	gas yield for CH_4 during the reaction with methane in the batch reactor
$\gamma_{CO,syn}$	gas yield for CO during the reaction with syngas in the batch reactor
$\gamma_{H2,syn}$	gas yield for H_2 during the reaction with syngas in the batch reactor
γ_v	gas conversion for volatiles
$\gamma_{v,i}$	conversion of gas i (i = CH_4, CO or H_2) from volatiles
γ_φ	overall gas conversion for solid fuels
Δp	pressure drop over the bed in the reactor, Pa
ε	ratio of volume expansion for full combustion of CH_4
κ	ratio of ($\xi·g$) and V_0
ξ	fraction of char gasification in the fuel reactor
$\varphi_{s,j}$	contact efficiency of bed material with char gasification products (j = c) or volatile components (j = v)
ψ	ratio between oxygen demand by char and the solid fuel for complete combustion
ω	mass-based conversion of the oxygen carrier in the batch reactor
ϑ	molar ratio between total oxygen consumed by H_2 and CO in syngas experiments
Ω_{OD}	oxygen demand
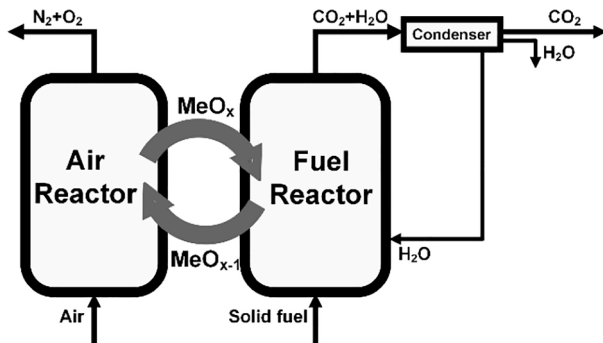
Fig. 1. Schematic layout of the CLC technology.

$$Solid\,fuel \rightarrow Char + Volatiles(CH_4, CO, H_2) \tag{R1}$$

$$Char + H_2O \rightarrow CO + H_2 + Ash \tag{R2}$$

$$CH_4 + MeO_x \rightarrow CO_2 + H_2O + MeO_{x-1} \tag{R3}$$

$$CO + MeO_x \rightarrow CO_2 + MeO_{x-1} \tag{R4}$$

$$H_2 + MeO_x \rightarrow H_2O + MeO_{x-1} \tag{R5}$$

$$MeO_{x-1} + Air \rightarrow MeO_x + N_2 + O_2 \tag{R6}$$
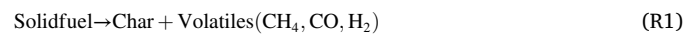
The oxygen carrier is a key for CLC, as it transfers the oxygen from combustion air to fuel in the fuel reactor [3]. Numerous works in the past decades have been dedicated to finding suitable oxygen carrier materials for CLC with gaseous and solid fuels [2,3]. In the case of solid

fuels, inexpensive natural minerals and industrial by-products are preferred considering the inevitable oxygen carrier loss with ash removal. The most extensively studied and demonstrated oxygen carriers are ilmenite [11–14], iron ore [15–18], manganese ore [19–26] and $CaSO_4$-based materials [27,28]. Among them, manganese ores have shown better reaction performance than ilmenite [22,23,29,30] and iron ores [23,30], and avoids the problem with sulfur emission from $CaSO_4$ [27,31,32]. In addition, there is a potential for gaseous O_2 release from manganese ores, a mechanism known as Chemical Looping with Oxygen Uncoupling (CLOU) [33], which means the fuel can burn with O_2 gas. This improves fuel conversion, as there is no need for steam gasification of the fuel. In this context, the cumulative operational experience with manganese ores in CLC pilots around the world exceeds 800 h [3]. Generally, most of the manganese ores studied have a small gaseous oxygen release [30,34]. Further, some ores show a noticeable promotion of char gasification as a result of catalytic effects of alkali impurities in the materials [23,35,36]. In several tests in continuous units, the conversion of intermediate components (CH_4, CO and H_2) was significantly enhanced as compared to ilmenite [20,22,24–26,37–39], which means less oxygen will be required for the oxy-polishing step [10,40,41]. On the other hand, high attrition rates have been observed in several cases, which would mean a shorter oxygen-carrier lifetime [42–44]. Adding foreign ions/supports [45,46] and sintering at high temperatures [21] can help to reduce attrition. In this context, a manganese ore, Elwaleed B, originating from Egypt, denoted as EB, with good reactivity and reasonably low attrition was demonstrated in a 10 kW_{th} unit burning biomass-based fuels [22]. Using this manganese ore, a decrease of 8–10% in oxygen demand was reached as compared to ilmenite, while the estimated lifetime was around 370–830 h, which would be sufficient for industrial systems [10].

Modelling of reactors is a powerful tool for the development of CLC technology. A number of mathematical, multiphase Computational Fluid Dynamics (CFD) and even analytical models were developed and successfully applied to continuous reactors with a thermal power of 0.5 kW_{th}-1 MW_{th} in recent years [47–55]. These models use kinetic equations to describe the chemical reactions and semi-empirical/theoretical fluid dynamics to depict the gas/solid distribution in the reactors. Usually, the computational time cost and accuracy are the major concerns for these models, considering large numbers of calculating cells might be required. In comparison to CFD models, macroscopic mathematical model can give results within minutes of computational time [47,51], while keeping relevant information and giving good accuracy. The macroscopic model is more straightforward and has been well applied for the design and optimization of 10–100 MW_{th} CLC plants [56,57]. Still, considering the limited experimental data available from larger units, and the fact that many parameters are unknown in this relatively new technology, the development of simplified modelling approaches could be valuable in order to identify importance of underlying parameters. Analytical modelling may in this regard be a useful tool. Such models are based on the analytical solution of differential equations considering reaction kinetics, fluid dynamics and mass balances [52,58]. An analytical model was demonstrated for gas conversion predictions in a 10 kW_{th} unit [58] and a 100 kW_{th} unit [52] for solid fuels, where the gas conversion was predicted as a function of oxygen carrier reactivity, solids inventory and gas flow. Analytical modelling, having the advantage of a high degree of transparency, could be an important tool for understanding and predicting CLC process better.

This work uses an analytical reactor model for the study of EB manganese ore oxygen carrier studied in recent 10 kW_{th} operation [22]. Reactivity and reaction rate with the fuel components (CH_4, CO and H_2) required by the model were determined by batch-reactor tests under fluidization conditions. Fluid dynamics and mass balances were considered, which together with the rates of gas–solid reactions and char gasification can predict gas conversion. From the analytical model, the rate of char gasification, contact efficiency of bed material with gasification products and volatiles in the 10 kW_{th} pilot were estimated.

2. Experiments

2.1. Oxygen carriers

Samples of fresh manganese ore "EB" and three used ones from a previous 10 kW_{th} operation [22], as well as ilmenite from another 10 kW_{th} operation campaign [59], were investigated in the current work. The used EB samples were from the initial, middle and final stages of the 42 h of operation in the 10 kW_{th} unit [22] and are denoted as Us1, Us2 and Us3 in this work. Among the 42 h of operation in the 10 kW_{th} reactor, 21 h involved the use of three biomass-based fuels at a temperature of 820–985 °C under steam fluidization [22]. As in the previous work [22], the fresh EB is composed of particles with a mean diameter of d50 = 183 μm after calcination, wet sieving and drying processes. The freshly calcined EB has a composition of around 24.8% Mn, 25.3% Fe, 8.1% Si and other minerals, as seen in Table 1. The ilmenite was used as a benchmark to compare with the EB ore. The original fresh calcined ilmenite before any tests mainly contains around 32.8% Fe, 25.0% Ti and 2.8% Si, as shown in Table 1. Since the ilmenite has undergone 21 h of operation with solid fuels in the 10 kW_{th} unit at a temperature of 879–992 °C [59], it is in an activated state and the chemical composition may be different from the fresh material, e.g. due to iron migration to surface [60–63].

2.2. Fuels

The main gas-phase fuel components in CLC processes are CH_4, CO and H_2. Thus, in this work, CH_4 and syngas containing 50% CO and 50% H_2 were employed for the reactivity tests in the batch reactor. The idea with these experiments is to retrieve reaction rate data which can be used in the modelling. These two fuels were initially stored in high-pressure cylinders. Prior to use, they were regulated to close to atmospheric pressure before being sent to the downstream reactor. The solid fuel used in the batch reactor experiments of this work is a char made by devolatilizing wood pellets at 1073 K under 100% N_2 environment in a batch reactor [64]. Therefore, the wood-pellet char generated is designated as "WPC", and it has around 93.5% carbon, <0.5% hydrogen and 3.0% oxygen. In the current work, the WPC char was added to a bed of EB particles fluidized by 100% N_2, to investigate the rate of gas-phase oxygen release.
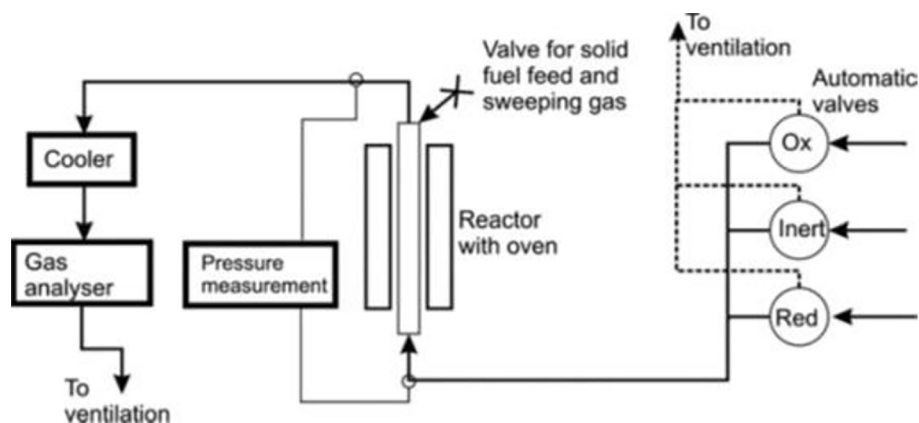
2.3. Batch fluidized-bed reactor setup

The reduction and oxidation cycles in the CLC process were performed by exposing the oxygen carrier alternately to fuel and oxidizing environment in a batch fluidized-bed reactor [65,66], as displayed in Fig. 2. The quartz reactor tube has a length of 820 mm and an inner diameter of 22 mm, which is surrounded by an electrically heated furnace. Bed materials were loaded on a porous quartz plate located inside the tube at around 370 mm above the bottom. Two thermocouples were placed at around 20 mm above and 10 mm below the porous plate to measure the temperatures for the bed and inlet-gas stream, respectively. To provide information about the fluidization state, the pressure drop over the bed was monitored by a transducer connecting between the top and bottom of the reactor [67,68]. Defluidization can be detected from loss of pressure fluctuations. Fluidization and fuel gases were introduced from the reactor bottom. These reacted with the bed material and then left via the reactor top. After steam condensation in the downstream cooler, the outlet gas was led to a gas analyzer (NGA 2000, Rosemount ™) to measure the concentrations of CH_4, CO, CO_2, H_2 and O_2 as well as the volumetric flow at a rate of one sampling point every two seconds. Among the measured gases, H_2 sometimes shows a delay or an inaccurate concentration as a result of the internal adjustment in the analyzer. This will affect some of the calculated parameters but can be corrected by proper data processing methods [69], as discussed in *Section 4* below. The temperature, gas concentration,

Table 1
Chemical composition for the fresh calcined EB and ilmenite (wt.%).

	Mn	Fe	Ti	Si	Ca	Mg	Al	K	Na
EB	24.83	25.33	0.09	8.13	2.32	0.93	0.97	0.43	0.39
Ilmenite	0.12	32.80	24.99	2.81	0.39	2.83	0.54	0.06	0.12

Fig. 2. Setup of the batch fluidized-bed reactor.

Table 2
Bed composition and reducing environment for different types of test.

Test type	Bed composition		Reduction environment		Fuel amount
	Oxygen carrier	Sand	N_2 flow	Fuel type	
CLOU	15 g	–	900 ml/min	–	–
CLOU	15 g	–	1200 ml/min	WPC	0.1 g
CLC	15 g	–	–	CH_4	345 ml/min
CLC	2 g	13 g	–	Syngas	450 ml/min

volumetric flow and pressure drop were regularly registered in a computer connected to a data logger.

2.4. Reaction conditions

In all the tests in the batch reactor, the temperature was set to 1223 K. The bed composition and oxygen carrier reduction environment for different types of test are summarized in Table 2. In the case of gaseous oxygen release, 15 g fresh EB, Us1, Us2 or Us3 were used as the bed material, while the fluidization agent was 100% N_2 at a flow rate of 900 ml/min. In addition to this, there are several cases conducted with N_2 as fluidization gas but using WPC char as the reduction agent. In these cases, around 0.1 g WPC accompanied with 300 ml/min sweep N_2 were injected from the reactor top (i.e. the "Valve for solid fuel feed and sweeping gas" in Fig. 2). The oxygen release was characterized by the gaseous O_2 concentration detected in N_2 as well as the rate of oxygen carrier conversion in WPC experiments derived from CO and CO_2 produced. In the tests with gaseous fuels, CH_4 with a flow of 345 ml/min or syngas with a flow of 450 ml/min was used as reduction agent, while different amounts of fresh EB, Us1, Us2, Us3 or ilmenite were used. For

CH_4, 15 g oxygen carrier was used in the bed, whereas a mixture of 2 g oxygen carrier and 13 g sand was used for syngas. Less oxygen carrier was used in the latter case to avoid full syngas conversion and thus to acquire data useful for evaluation [70]. For both CH_4 and syngas, the reduction time was set to 20 s to lower the risk of defluidization and/or agglomeration caused by deep reduction [67,68]. The oxidation step was performed with 5% O_2 following 180 s of purge with N_2.

3. Models

3.1. Solid fuel pyrolysis

To compare with the experimental results in the recent 10 kW_{th} operation [22], the same fuels "BP" and "SWC" were used for the analytical modelling. BP is steam cured wood pellets, called "black pellets", and contains 18.7% fixed carbon and 74.2% volatiles, while SWC is a commercial Swedish wood char and has 73.9% fixed carbon and 16.7% volatiles, as shown in Table 3.

From the fuel analysis, it is possible to predict the contents of gas components after pyrolysis using an empirical model [71], as seen in Eq. (1). In this simple model, the constants in the left square matrix were derived from large amounts of experimental data, while the right column matrix were based on fuel composition. The constants in the empirical model were obtained from coal pyrolysis and adapted to use for biomass-based fuels [71]. After solving the matrix equation, the pyrolysis products as displayed in the middle column matrix can be obtained, which gives the weight percentages of coke, tar and gas constituents. To be used in CLC process, the C_2H_6 and tar calculated from Eq. (1) were further reformed and gasified in the model to CO and H_2 which added to the model-derived CH_4, CO and H_2 representing the

Table 3
Fuel analysis and model-predicted fractions of volatile combustibles.

	Proximate (wt.%, as received)				Ultimate (wt.%, dry and ash free)					Volatile combustibles [a] (wt.%, as received)		
	FC	V	M	A	C	H	N	S	O [b]	CH_4	CO	H_2
BP	18.7	74.2	6.9	0.3	53.5	6.0	0.1	0.0	40.3	7.8	55.9	2.6
SWC	73.9	16.7	3.9	5.5	86.9	3.2	0.4	0.0	9.5	3.9	7.3	1.2

[a] calculated from the empirical model in Eq. (1).
[b] by difference.

volatile combustibles [51]. The other gas components (CO_2, H_2O, NH_3 and H_2S) were not considered in the present work, as they are not combustibles or only present in trace fractions. As seen in Table 3, BP has a much higher fraction of the combustible gases CH_4, CO and H_2 than SWC, which is consistent with the higher volatiles content in the proximate analysis. Meanwhile, CO and CH_4 are the more dominant gases in the volatiles according to the pyrolysis model, see Table 3, which might be a result of C_2H_6 reforming and tar gasification.

$$\begin{pmatrix} 0.9632 & 0.75 & 0.8 & 0.4286 & 0.2727 & 0.8342 & 0 & 0 & 0 & 0 \\ 0.0059 & 0.25 & 0.2 & 0 & 0 & 0.0679 & 1 & 0.1111 & 0.1765 & 0.0588 \\ 0.0036 & 0 & 0 & 0.5714 & 0.7273 & 0.0652 & 0 & 0.8889 & 0 & 0 \\ 0.0129 & 0 & 0 & 0 & 0 & 0.0197 & 0 & 0 & 0.8235 & 0 \\ 0.0144 & 0 & 0 & 0 & 0 & 0.0130 & 0 & 0 & 0 & 0.9412 \\ 1 & 0 & 0 & 0 & 0 & 0 & 0 & 0 & 0 & 0 \\ 0 & 1 & 0 & 0 & 0 & 0 & 0 & 0 & 0 & 0 \\ 0 & 0 & 1 & 0 & 0 & 0 & 0 & 0 & 0 & 0 \\ 0 & 0 & 0 & 1 & 0 & 0 & 0 & 0 & 0 & 0 \\ 0 & 0 & 0 & 0 & 1 & 0 & 0 & 0 & 0 & 0 \end{pmatrix} \cdot \begin{pmatrix} \text{Coke} \\ CH_4 \\ C_2H_6 \\ CO \\ CO_2 \\ \text{Tar} \\ H_2 \\ H_2O \\ NH_3 \\ H_2S \end{pmatrix} = \begin{pmatrix} C \\ H \\ O \\ N \\ S \\ 1\text{-V} \\ 0.82 \cdot H \\ 0.15 \cdot H \\ 0.59 \cdot O \\ 0.31 \cdot O \end{pmatrix} \quad (1)$$

3.2. Analytical model for fuel reactor

3.2.1. Model description

In previous works, an analytical model for the fluidized-bed reactor was developed and adapted for simulating the gas conversion in a 10 and a 100 kW_{th} unit [52,58]. This model considers an even distribution of oxygen carrier and char in the bed, as described in Fig. 3, where the total oxygen carrier mass is m_{tot}. Fluidization and reactive gas comprised of H_2O and volatiles has a total volumetric flow of V_0, which enters the bed from the bottom. The volatile components are converted by the bed material, while their conversion is assumed to preserve the total inlet flow V_0, meaning the volume expansion during volatiles combustion is not considered due to the low fraction of CH_4 as seen in Table 3. Thus, the outgoing gas at the bed surface is composed by two streams, i.e. V_g and V_0. The V_g represents the volumetric flow of gas from char gasification, which can be a mixture of CO, H_2, CO_2 and/or H_2O depending on their extents of conversion. Assuming a linear increase of V_g along bed height [52,72], the total gas flow V_m at coordinate m can be written as Eq. (2).

$$V_m = V_0 + V_g \frac{m}{m_{tot}} \quad (2)$$

Inside the reactor, char gasification as well as gas–solid reactions between fuel components (CH_4, CO and H_2) and oxygen carrier were considered·H_2O serves as a gasification agent and converts the char to H_2 and CO. The amount of CO and H_2 generated from char gasification $dn_{i,g}$ in the differential element dm was calculated by Eq. (3).

$$dn_{i,g} = C_{i,g} V_g \frac{dm}{m_{tot}} \quad (3)$$

where $C_{i,g}$ is the concentration of gas i (i = CO or H_2) in the mixture of gas products from gasification before any reaction with the oxygen carrier bed.

The fuel components CH_4, CO and H_2 from both volatiles and char gasification are mainly converted by reacting with the oxygen carrier. In this work, a gas–solid reaction with a first-order reaction regime was used to describe the conversion of these components. Accordingly, the consumption, $dn_{i,r}$, of gas i (i = CH_4, CO or H_2) via gas–solid reactions in the dm element is given by Eq. (4).

$$dn_{i,r} = -k_{F,i} C_{i,m} dm \quad (4)$$

where $k_{F,i}$ is a mass-based rate constant, determined by tests in the batch reactor, as seen in *Section 4*, and $C_{i,m}$ represents the concentration of component i at coordinate m in the bed.

3.2.2. Partial pressure of CH_4, CO and H_2

In order to calculate the gas conversion for CLC process, the un-converted gases (CH_4, CO and H_2) leaving the reactor are important to determine. Hence, based on a mass balance in the dm element, the differential equation Eq. (5) can be formulated and used to calculate the concentration change, $dC_{i,m}$, in the differential element.

$$dC_{i,m} = \frac{1}{V_m} \left(dn_{i,g} + dn_{i,r} - C_{i,m} V_g \frac{dm}{m_{tot}} \right) \quad (5)$$

where $dn_{i,g}$ and $dn_{i,r}$ are the generation and consumption of gas i (i = CH_4, CO or H_2) as a result of char gasification and reaction with the oxygen carrier, given by Eqs. (3) and (4), respectively.

Further processing of Eq. (5) was done to get the partial pressure p_i for gas i (i = CH_4, CO or H_2) by applying the ideal gas law ($pV = nRT$) and atmospheric pressure in the reactor. In this case, Eq. (5) is converted to the following differential equation.
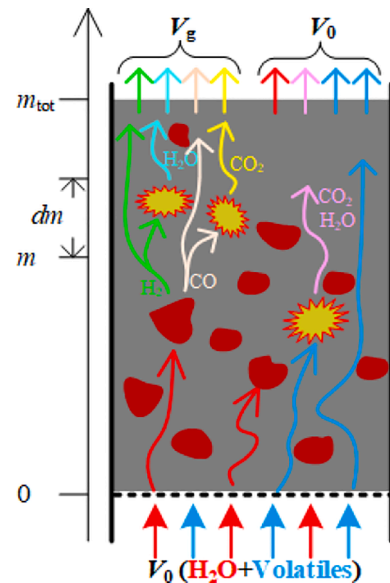

Fig. 3. Description of reactions and gas flows considered in the analytical model, red area (■) represents the char distribution, gray area (■) is for oxygen carrier bed and star (★) shows the gas-oxygen carrier reactions. The arrows in the bed indicate the routes for gas transfer and conversion and the left arrow shows the coordinate m with the differential element dm much smaller (≪) than m

$$\frac{dp_i}{dm} = \frac{1}{m_{tot} + \kappa m}\left(\frac{-k_{F,i}m_{tot}}{V_0}p_i + \kappa p_i + (1 + \kappa)p_{i,g}\right) \tag{6}$$

where κ is the ratio of ξV_g and V_0, and the symbol ξ indicates the fraction of char gasified in the fuel reactor and $p_{i,g}$ is the partial pressure of gas component i ($i = CO$ or H_2) from char gasification. The value of ξ will be determined by fitting with experimental results from the previous 10 kW_{th} operation [22].

Differential equation Eq. (6) has an analytical solution, which gives the partial pressure $p_i(m)$ of gas i ($i = CH_4$, CO or H_2) at coordinate m and takes a general form as Eq. (7) below.

$$p_i(m) = \frac{1}{\alpha_i + \kappa}\left(p_{i,g}(1 + \kappa) + (p_{i,0}(\alpha_i + \kappa)\right.$$
$$\left. - p_{i,g}(1 + \kappa))\left(\frac{m_{tot} + \kappa m}{m_{tot} + \kappa m_0}\right)^{-\alpha_i/(\kappa-1)}\right) \tag{7}$$

where $p_{i,0}$ is the partial pressure of component i in gas entering the reactor, and the symbol α_i is a dimensionless number, as shown in Eq. (8a).

$$\alpha_i = \varphi_{s,j}\frac{k_{F,i}m}{V_0} \tag{8a}$$

where $\varphi_{s,j}$ is the contact efficiency of bed material and char gasification products ($j = c$) or volatiles ($j = v$), with $\varphi_{s,c} = 0.9$ based on the high conversion of SWC char, with the oxygen demand as low as 2.6%, in the previous 10 kW_{th} experiments [22] and agreeing with the results from previous works [52,53] and $\varphi_{s,v}$ is determined by fitting with the 10 kW_{th} experiments [22].

Considering a reactor tube with A_c as the inner cross-section area, Δp as the pressure drop over the bed while CI and T are the circulation index [73] and operation temperature, the α_i can be calculated by Eq. (8b) considering the effects of solids circulation index and operation temperature [52] using exponential factors n_{CI} and n_T, respectively.

$$\alpha_i = \varphi_{s,j}\frac{A_c k_{F,i}\Delta p}{gV_0}\left(\frac{CI}{CI_0}\right)^{n_{CI}}\left(\frac{T}{T_0}\right)^{n_T} \tag{8b}$$

where the exponents n_{CI} and n_T are determined by fitting with experimental results. Initial values CI_0 and T_0 are from experimental averages, and g is the acceleration of gravity.

The final gas conversion is obtained from the partial gas pressures at the bed surface according to Eq. (7). To do this, the general solution above is divided into two cases: (a) only char as fuel in the bed and (b) only gases as fuel in the bed. Therefore, the following Eqs. (9) and (10) were used to describe the partial pressure of gas i for char ($i = CO$ or H_2) and volatile combustibles ($i = CH_4$, CO or H_2), respectively, at the bed surface.

$$p_i(\alpha_i) = \frac{p_{i,g}}{\alpha_i + \kappa}\left((1 + \kappa) - (1 + \kappa)^{-\alpha_i/\kappa}\right) \tag{9}$$

$$p_i(\alpha_i) = p_{i,0}e^{-\alpha_i} \tag{10}$$

3.2.3. Gas conversion

From the expressions of partial pressure of gas component leaving the bed surface in Eqs. (9) and (10), the conversion, $\gamma_{c,i}$ for species i from char gasification ($i = CO$ or H_2) and $\gamma_{v,i}$ from volatiles ($i = CH_4$, CO or H_2), can be calculated using Eqs. (11) and (12), respectively.

$$\gamma_{c,i}(\alpha_i) = 1 - \frac{(1 + \kappa) - (1 + \kappa)^{-\alpha_i/\kappa}}{\alpha_i + \kappa} \tag{11}$$

$$\gamma_{v,i}(\alpha_i) = 1 - e^{-\alpha_i} \tag{12}$$

The above obtained conversions for components i ($i = CH_4$, CO and H_2) are further combined to predict the gas conversion for char and

volatiles. Considering that the same amount of oxygen is needed for full oxidation of CO and H_2, the gas conversion for char can be calculated as Eq. (13).

$$\gamma_c = 0.5\gamma_{c,CO} + 0.5\gamma_{c,H_2} \tag{13}$$

Similarly, the gas conversion for the volatiles can be obtained from the conversion of CH_4, CO and H_2 using the ratios a, b and c for CH_4, CO and H_2 in the volatiles, as seen in Eq. (14).

$$\gamma_v = a\gamma_{v,CH_4} + b\gamma_{v,CO} + c\gamma_{v,H_2} \tag{14}$$

where the a, b and c denote the fraction of total oxygen demand relating to CH_4, CO and H_2. Thus, $a + b + c = 1$ and a, b and c were derived from the volatile combustibles in Table 3. Stoichiometrically, four moles oxygen are needed for complete combustion of one mole CH_4, while one is needed for CO and H_2. The ratio of oxygen required for CH_4, CO and H_2 over the corresponding total amount in volatiles is denoted as a, b and c, respectively. For example, in the case of BP fuel in Table 3, 7.8% CH_4, 55.9% CO and 2.6% H_2 were calculated from the model in Eq. (1), which correspond to 0.5 mol CH_4, 2 mol CO and 1.3 mol H_2 in 100 g BP fuel. These are translated to 2 mol, 2 mol and 1.3 mol of oxygen atom required for complete combustion of CH_4, CO and H_2, respectively. So, the values for BP were calculated as $a = 0.38$ for CH_4, $b = 0.38$ for CO and $c = 0.24$ for H_2, while they were 0.53, 0.14 and 0.33, respectively, for the SWC char.

Finally, the gas conversion for char and volatiles obtained by Eqs. (13) and (14) need to be further weighted together to form the overall gas conversion γ_φ for the solid fuel. As shown in Eq. (15), the overall gas conversion depends not only on the oxygen demand ratio ψ for complete combustion of char in the fuel, but also on the char gasification fraction ξ.

$$\gamma_\varphi = \xi\psi\gamma_c + (1 - \xi\psi)\gamma_v \tag{15}$$

where ψ is 0.36 and 0.88 for BP and SWC, respectively, based on the fuel analysis in Table 3, and the value of ξ is determined from the 10 kW_{th} experimental results.

With the overall gas conversion, the oxygen demand Ω_{OD}, showing the ratio of theoretical amount of oxygen required for complete combustion of unconverted fuel-reactor gases (CH_4, CO and H_2) over the oxygen needed for complete fuel combustion, is obtained from Eq. (16).

$$\Omega_{OD} = 1 - \gamma_\varphi \tag{16}$$

3.2.4. Inputs and outputs

The main inputs to the analytical model are reaction rate constants, reactor geometry, total pressure drop over the bed as well as the base operation conditions as shown in Table 4 below. Since the reaction rate were obtained with the batch-reactor tests at 1223 K, the base fuel-reactor temperature T_0 in the analytical model was set to 1223 K. For the other parameters, the base values are the averages from stable operations in two recent 10 kW_{th} campaigns [22,59], which are shown in Table 4 for different oxygen carrier and fuel pairs.

The outputs from the reactor model are the gas conversion of component i ($i = CH_4$, CO or H_2) calculated by Eqs. (11) and (12) for char and volatiles, the gas conversion for char and volatiles via Eqs. (13) and (14) as well as the overall gas conversion from Eq. (15). Among these outputs, the overall gas conversion γ_φ is the main focus in the

Table 4
Base values to be input for the analytical model.

	Fuel (-)	T_0 (K)	CI_0 (Pa· (m³/s))	V_0 (10^{-4} m³/s)	Δp (Pa)	V_g (10^{-4} m³/s)
EB	BP	1223	1.53	8.72	5252	2.30
EB	SWC	1223	3.97	8.36	5366	5.29
Ilmenite	BP	1223	6.49	7.24	6032	3.46
Ilmenite	SWC	1223	3.14	6.80	4678	5.29

present work.

4. Data evaluation

Using the volumetric flow measured by the gas analyzer, the total gas molar flow $\dot{n}_{out}$ from the batch reactor was obtained by applying a factor from calibration. Then, the mass-based conversion ω of the oxygen carrier bed as a function of reaction time t is calculated by Eqs. (17) and (18) for CH_4 and syngas [34], respectively. The oxygen carrier conversion during the CLOU tests with WPC char is also calculated by Eq. (18) but with $x_{H2} = 0$, considering that 93.5% of this char is composed by carbon, see *Section 2.2* above.

$$\omega = 1 - \int_{t_0}^{t} \frac{\dot{n}_{out} M_O}{m_{ox}} (4x_{CO_2} + 3x_{CO} - x_{H_2}) dt \tag{17}$$

$$\omega = 1 - \int_{t_0}^{t} \frac{\dot{n}_{out} M_O}{m_{ox}} (2x_{CO_2} + x_{CO} - x_{H_2}) dt \tag{18}$$

where t_0 corresponds to the time at the beginning of the reaction, M_O and m_{ox} are the molar mass of atomic oxygen and the mass of oxygen carrier used in the reactor, respectively. x_i represents the fraction of gas i ($i = CO_2$, CO or H_2) measured by the gas analyzer.

Gas yield indicates the extent of fuel conversion to CO_2, which was calculated from the measured gas concentrations, similar to previous works [74,75]. The gas yield, from CH_4 in the methane and from CO in the syngas, was obtained with Eqs. (19) and (20), respectively.

$$\gamma_{CH_4,CH_4} = \frac{x_{CO_2}}{x_{CH_4} + x_{CO} + x_{CO_2}} \tag{19}$$

$$\gamma_{CO,syn} = \frac{x_{CO_2}}{x_{CO} + x_{CO_2}} \tag{20}$$

Using these gas yields, the mass-based rate constants for CH_4 and CO can be subsequently calculated by Eqs. (21) and (22), respectively. These equations consider first-order reactions between the oxygen carrier and the fuel components at atmospheric pressure [76,77], as the oxygen uncoupling with gaseous O_2 release is not significant for the EB ore as discussed in *Section 5.1*. The first-order assumption is in consistence with literature data [51,52,58,77,86] obtained in CLC reacting environment with various oxygen carriers, where the reaction orders are one or close to one for CH_4, CO and H_2.

$$k_{F,CH_4} = \frac{V_{CH_4}\left(-(1+\varepsilon)\ln(1 - \gamma_{CH_4,CH_4}) - \varepsilon\gamma_{CH_4,CH_4}\right)}{m_{ox}} \tag{21}$$

$$k_{F,CO} = \frac{V_{syn}\left(-\ln(1 - \gamma_{CO,syn})\right)}{m_{ox}} \tag{22}$$

where V_{CH4} and V_{syn} are the inlet volumetric inlet flows of CH_4 and syngas, respectively. The symbol ε represents the volumetric expansion ratio for full combustion of CH_4 with $\varepsilon = 2$.

Since the rate constant for H_2 is sensitive to the measured H_2 concentration and the later can be incorrectly adjusted by the analyzer, the $k_{F,H2}$ cannot be calculated with a similar method in Eq. (22). In this case, a molar ratio, ϑ, between the total oxygen consumed by H_2 and CO in the syngas was used to calculate the rate constant for H_2 [69], see Eq. (23). The value of ϑ was obtained by knowing the areas below the H_2 concentration curve and the CO concentration curve, i.e. integration of these concentration curves over reaction time, as well as the amount of H_2 and CO entering the reactor. Typically, the ϑ changed slightly in the range of 1.1–1.2 as a function of cycles, and this was considered during the calculation of rate constant for H_2.

$$k_{F,H_2} = \vartheta k_{F,CO} \tag{23}$$

5. Results and discussions

5.1. Gaseous oxygen release

5.1.1. Progress of O_2 concentration in N_2 environment

The oxygen release from EB samples was tested in 100% N_2 environment immediately after the oxidation process with 5% O_2. Meanwhile, the results for using sand as inert bed [78] as well as a CuO/Al_2O_3 material [33], typical for CLOU, were employed for comparison purposes, as shown in Fig. 4. In the case of sand, the concentration of O_2 decreased rapidly to zero within 25 s from $t = 15$ to 40 s as the fluidization gas was switched from 5% O_2 to 100% N_2. Because the sand is inert for oxygen release, the corresponding O_2 curve can be considered as a blank reference. In comparison to the sand bed, manganese ore has slower decrease in O_2 concentration and longer non-zero O_2 concentration duration (>100 s). This shows the capability of gaseous O_2 release from the manganese ore.

In Fig. 4, the O_2 release from Fresh EB, Us1, Us2 and Us3 is compared. The three used EB samples show a slightly higher O_2 concentration and a longer duration than the fresh material, although all the concentrations from these samples are lower than 0.5% after around $t = 50$ s. It is not clear if there is an activation of the EB ore for gaseous oxygen release, however, the capability of O_2 release is confirmed for both the fresh and used materials, consistent with the 10 kW_{th} results [22]. The oxygen release from EB ore is also compared with a CuO/Al_2O_3 oxygen carrier [33] under similar reaction conditions. Obviously, the concentration of O_2 from the manganese ore is much lower, i.e. < 0.5% versus 2–4% at the same temperature of 1223 K [33,79]. Therefore, the manganese ore can be classified as a CLOU material with low oxygen release.

5.1.2. Rate of oxygen release

Under inert environment, e.g. in N_2 fluidization, the O_2 concentration from oxygen release may be limited by the thermodynamic equilibrium maximum value [33,79,80]. The addition of solid fuel consumes instantaneously the generated O_2, removing the equilibrium barrier and thus shows the oxygen release rate in the absence of gas phase oxygen [33,34,81]. This is also more applicable for a real system, where it is expected that O_2 concentration in the bulk is very low [33,82]. A typical cycle using WPC as solid fuel in N_2 atmosphere is shown in Fig. 5, where the first 12 min corresponds to the reduction step which is followed by
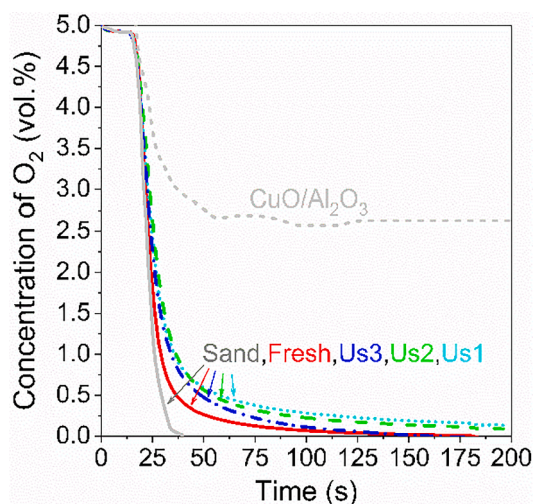

Fig. 4. Concentration of O_2 as a function of time after switching from 5% O_2 to 100% N_2 at a reactor temperature of 1223 K: comparison of Fresh EB, Us1, Us2 and Us3. Sand data from previous work [78] and CuO/Al_2O_3 results from another work [33] are also presented for comparison.
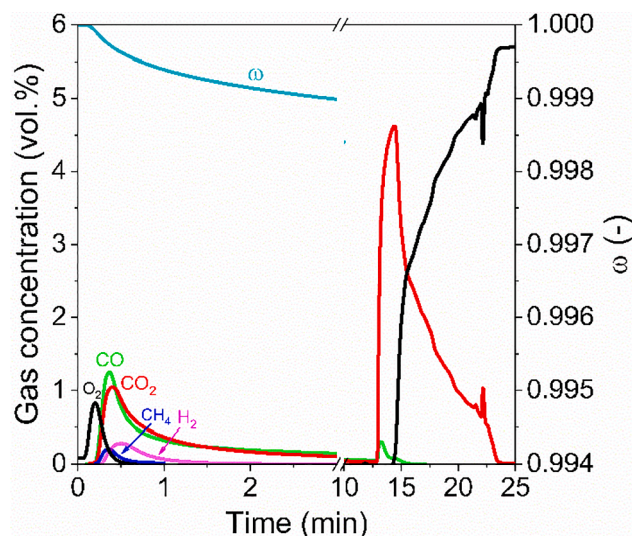
Fig. 5. Use of WPC char to study the oxygen release from EB ore: gas concentrations and mass-based oxygen carrier conversion (ω) as a function of time in a typical cycle with fresh EB at 1223 K. Reduction fluidization gas: 100% N_2, oxidation gas: 5% O_2.

oxidation with 5% O_2. When the WPC was introduced, peaks of all the measured gas components were detected, of which CH_4 and H_2 might be from the little residual volatiles in the char. The CO_2 and CO rising at the same time are a result of both a minor devolatilization and oxidation by the gaseous oxygen released from the oxygen carrier, while the peak of O_2 might be caused by the effects of solid fuel injection and/or the exothermic fuel combustion [9]. After the initial 1 min, only CO and CO_2 were observed during the reduction of oxygen carrier, which shows a continuation of solid fuel combustion by the insufficient O_2 from oxygen uncoupling. In the beginning of the oxidation period, high concentrations of CO_2 and small amount of CO indicate a low conversion of WPC during the previous reduction stage.

The rate of O_2 release is also described in Fig. 5 by the mass-based conversion ω of the oxygen carrier as a function of reaction time. Higher degree of reduction, i.e. a lower ω value, means that more oxygen has been transferred to the gas phase for fuel oxidation, thus a more reactive oxygen carrier with respect to CLOU. However, the EB

manganese ore only reaches $\omega = 0.999$. The average rate of oxygen release from the manganese ore is at a level of 0.01–0.015%/min, which is only 1% of the reaction with CH_4 and $< 1‰$ of the reaction with syngas as seen in *Section 5.2.2*. Thus, the gaseous O_2 release from the EB ore is small, and the CLOU effect can be neglected, which motivates the use of first-order reactions for EB with CH_4 and syngas. This is significant for the calculation of reaction rate constants and the analytical modelling under the assumption of first-order reaction regime.

5.2. Reactivity with gaseous fuels

5.2.1. Reaction progress

Gas concentrations in a typical redox cycle for the EB ore with CH_4 or syngas are presented as a function of reaction time in Fig. 6. Although the reduction time was set to 20 s, the gas concentration profiles last up to around 40 s, which is a result of gas back-mixing in the reactor, cooler and pipes leading to the gas analyzer, and a normal phenomenon in non-ideal reactors [83]. In the case of CH_4 in Fig. 6(a), the main gas leaving the reactor is unconverted CH_4 which is as high as 70%, whereas CO_2 and CO are below 15%, indicating a low reactivity of EB towards CH_4. There was no H_2 detected during the reduction, which might be a result of the full conversion of this intermediate component, considering its high reactivity. It is noted that although a significant fraction of CH_4 was not converted, there was no carbon deposition during the reduction step, because no carbonaceous gas was detected in the following oxidation. For the syngas in Fig. 6(b), the H_2 concentration is believed to be incorrectly adjusted by the gas analyzer, thus the initial H_2 concentration is slightly higher than CO, which was considered during the data processing, as seen in *Section 4*. Despite this, it is obvious that a much better conversion of syngas was achieved in comparison to CH_4, as the major gas leaving the reactor was CO_2 while the total peak concentration of CO and H_2 was only around 25%. Thus, much higher conversion was reached with syngas, despite a much lower amount of active material, 2 g instead of 15 g in the bed. Considering the equal concentrations of CO and H_2 in the inlet syngas (50% CO and 50% H_2), the lower residual H_2 indicates a higher reactivity of this component with EB than CO. The slower oxidation after syngas reduction as compared to CH_4 reduction is a result of higher degree of EB reduction in the former case, i.e. 0.955 for syngas versus 0.995 for CH_4. Agglomeration and defluidization of the bed were not observed during any cycle with CH_4 or syngas.
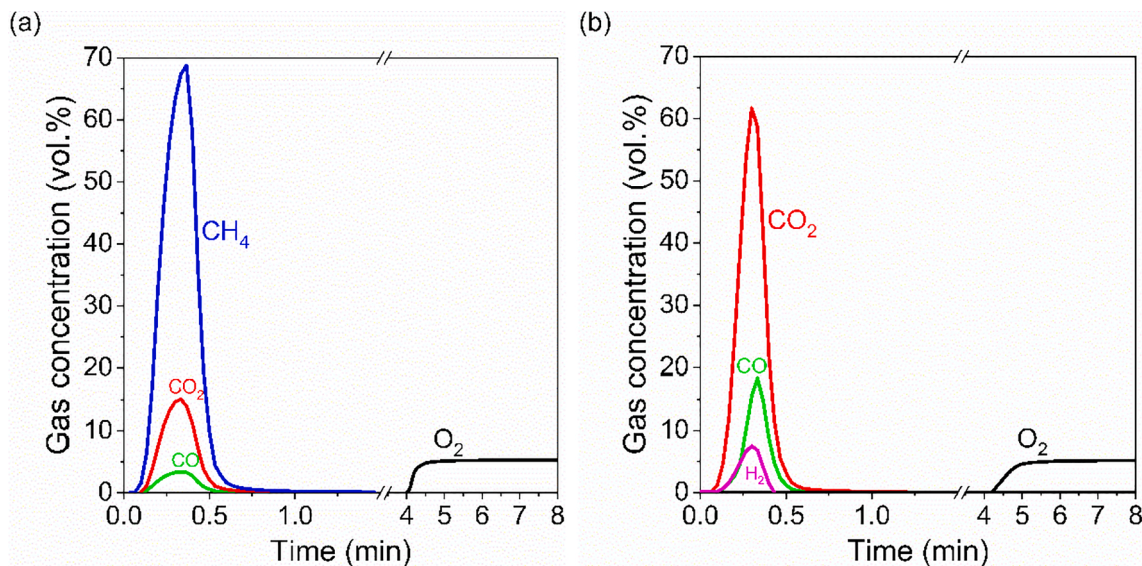

Fig. 6. Gas concentration for (a) CH_4 and (b) syngas (50% CO + 50% H_2), as a function of reaction time in a typical redox cycle with fresh EB oxygen carrier at a temperature of 1223 K.

5.2.2. Rate of oxygen carrier conversion

The rate of oxygen carrier conversion, $d\omega/dt$, as a function of mass-based conversion during the reaction with CH_4 or syngas is shown in Fig. 7. Generally, the rate increases significantly at the initial conversions and then remains at a relatively high value in the middle intervals of conversion, and finally declines quickly to a certain value as the fuel feeding is stopped. These rapid changes in the beginning and the end of reaction are attributable to the back mixing in the reactor as well as in the lines leading to and from the reactor [83].

In Fig. 7(a), the rate for fresh EB in various cycles with CH_4 and syngas is presented. Here the reaction rate increases slightly with rising cycle number. Despite this, it is hard to say if the material is activated or not in cycles, as differences are small. Nevertheless, it is clear that the syngas has much higher reactivity than CH_4, as a 7–10 times higher value for $d\omega/dt$ was achieved with syngas, leading to a higher degree of reduction of the EB material with syngas, reaching a ω as low as 0.955 as compared to above 0.995 for CH_4. The effect of operation in the 10 kW_{th} CLC unit [22] was also assessed by comparing the reaction rate of Fresh EB, Us1, Us2 and Us3 samples with CH_4 and syngas, see Fig. 7(b). For CH_4, the Fresh, Us2 and Us3 show similar reactivity, whereas Us1 has a somewhat higher reaction rate. Also, for syngas the difference is small, with Fresh and Us3 showing slightly higher reaction rate. Therefore, it can be concluded that the EB ore has a stable reactivity with CH_4 and syngas.

5.2.3. Comparison of EB with ilmenite

In Fig. 8, the gas yields from CH_4 in methane and CO in syngas are shown as a function of conversion for EB and ilmenite. The gas yield falls with the increasing oxygen carrier conversion for both CH_4 and CO. In the case of CH_4, EB ore has a gas yield of 0.27–0.15 as the conversion decreases from 1 to 0.996, which is around 20–40% higher than ilmenite. Using syngas as the fuel, the EB ore has a gas yield of higher than 0.76 from CO with the conversion varying in the range of 1–0.96, which is around 60% higher than the ilmenite. The higher gas yield for EB both with CH_4 and syngas is consistent with the lower oxygen demand for EB in the previous 10 kW_{th} operation [22].

5.3. Apparent rate constant

Fig. 9(a) shows the rate constant for CH_4, CO and H_2 as a function of the mass-based oxygen carrier conversion for EB and ilmenite. CH_4 has the lowest reactivity with a rate constant smaller than $0.2 \cdot 10^{-3} \, m^3/(kg \cdot s)$
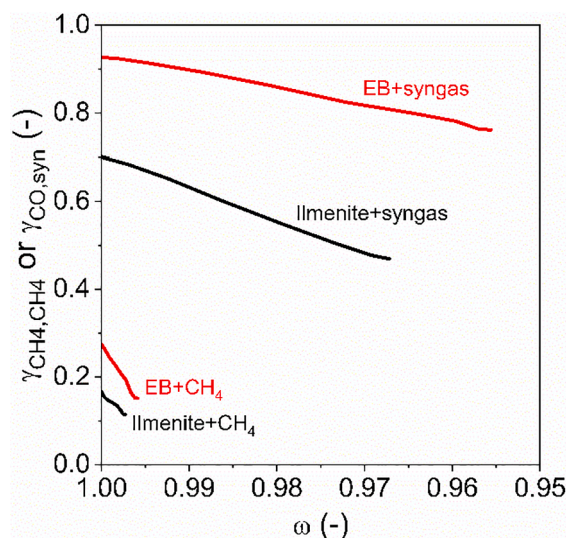

Fig. 8. Gas yield from CH_4 in methane and CO in syngas as a function of oxygen carrier conversion for using EB (Us3) and ilmenite as the active bed at 1223 K.

at all solid conversion levels for both EB and ilmenite, while the former is more reactive. In the case of CO and H_2, the rate constant for EB is much higher than that for CH_4, while the rate constant for H_2 is always higher than for CO. Compared to EB ore, the ilmenite shows a lower reactivity of all the gas components (CH_4, CO and H_2).

Using the oxygen carrier conversion of 0.98 for syngas and 0.998 for CH_4 as an example, the rate constant for CH_4, CO and H_2 is plotted as a function of cycle number in Fig. 9(b), where the variation in reactivity for EB and ilmenite can be evaluated and further compared. For the EB material, the rate constant decreases slightly in the first 3–4 cycles and then becomes relatively stable for CH_4, CO and H_2. This behavior suggests a reactivity decrease and stabilization of the manganese ore during the first cycles with CH_4 and syngas [30]. On the contrary, for ilmenite a clear increase in the rate constant for CH_4, CO and H_2 is seen in the cycles with both CH_4 and syngas. This activation behavior for ilmenite is commonly known in CLC processes using gaseous [60,61] and solid fuels [62]. For both EB and ilmenite, a stable rate constant is seen in the final cycles. Thus, EB has a higher reactivity than ilmenite with CH_4, CO and H_2.
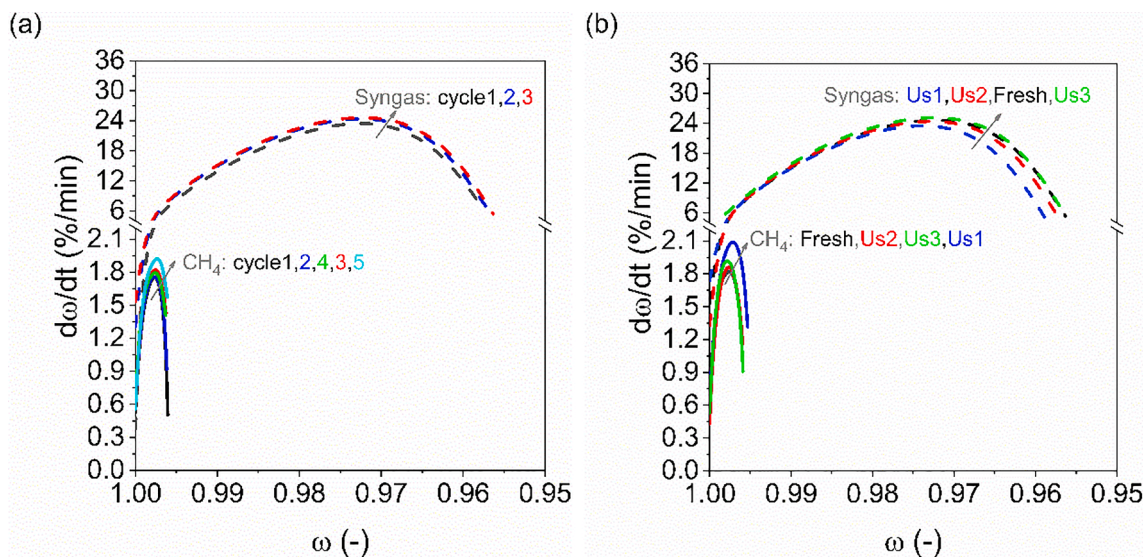

Fig. 7. Oxygen carrier conversion rate $d\omega/dt$ as a function of mass-based conversion ω during the reaction with CH_4 or syngas: (a) first cycles with fresh EB ore and (b) stable cycles with Fresh, Us1, Us2 and Us3 EB manganese ore at 1223 K.
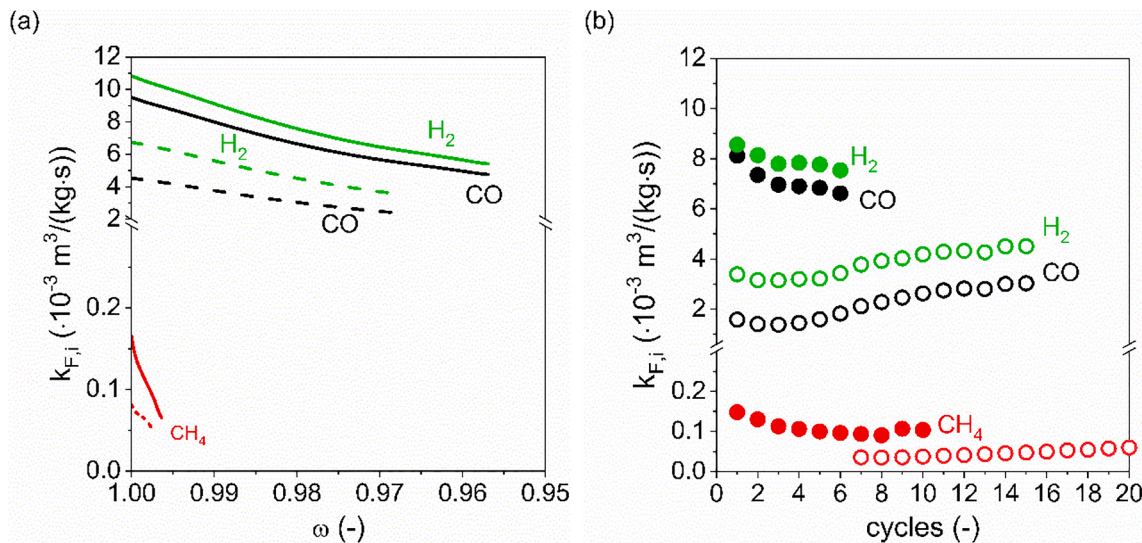
Fig. 9. (a) Typical rate constant as a function of mass-based conversion for CH$_4$ (—, – –), CO (—, - -) and H$_2$ (—, – –) using EB (Us3) (continuous lines) and ilmenite (dash lines) and (b) Rate constant as a function of cycle number with CH$_4$ (●, ○), CO (●, ○) and H$_2$ (●, ○) using EB (Us3) (filled symbols) and ilmenite (void symbols), CO and H$_2$ data are for $\omega = 0.98$ and CH$_4$ data for $\omega = 0.998$. The rate constant for CH$_4$ with ilmenite before cycle 7 are not available because conversion did not reach 0.998.

As observed in Fig. 9(a), the rate constant changes with the oxygen carrier conversion. For the analytical model, adequate rate constant data are needed. According to previous works [84,85], an oxygen carrier conversion variation of around $\Delta\omega = 0.02$ should be assured in the CLC system to maintain sufficient oxygen transfer and heat balance. Therefore, the oxygen carrier conversion of 0.98 is considered for selecting the rate constants for CO and H$_2$, whereas a value corresponding to the conversion of 0.998 is used for CH$_4$ because of the limited reduction degree of the oxygen carrier. As seen in Fig. 9(b), the reactivity decreased gradually to relatively stable values after some cycles. The rate constants from the last stable cycles were selected for use in the analytical model. The selected rate constants for CH$_4$, CO and H$_2$ with EB or ilmenite are from cycle 10 with methane and cycle 6 with syngas and listed in Table 5.

5.4. Fitting the analytical model with 10 kW$_{th}$ experiments

A value of $\varphi_{s,c} = 0.90$ has been proven reasonable for the contact efficiency of gasification products with the oxygen carrier in previous work [52] and is consistent with high conversion of SWC char in the 10 kW$_{th}$ experiments with an oxygen demand as low as 2.6% [22]. Thus, this value is also used in the current work for the analytical model. The parameters, ξ for gasification fraction of char and $\varphi_{s,v}$ for the contact efficiency of volatiles and bed, are determined by fitting with experimental results. According to the 10 kW$_{th}$ operation [22], the losses of char from BP or SWC are all lower than 2%, thus a high ξ should be expected, while a low $\varphi_{s,v}$ can be foreseen as big proportions of volatiles were unconverted. Moreover, these three parameters are not affected by the reactivity of oxygen carrier or fuel components, thus for all the solid fuels in the same reactor they should be kept at the same values. In this

case, the values of ξ and $\varphi_{s,v}$ were determined as 0.98 and 0.20 for both BP and SWC with EB or ilmenite to have a good fitting with the experimental data. Using these values, the oxygen demand for BP and SWC is predicted and compared with experimental results, as seen in Fig. 10(a) for EB and Fig. 10(b) for ilmenite. The modelling results show somewhat underestimation for "EB + BP", "Ilmenite + BP", "Ilmenite + SWC" and overestimation for "EB + SWC" experimental data. And the tendency of oxygen demand variation can be well predicted by the analytical model, which means the values of these parameters (ξ, $\varphi_{s,c}$ and $\varphi_{s,v}$) have a good sensitivity over different operation conditions.

Values for n_{CI} and n_T were obtained by fitting with experiments. Using the values for ξ and $\varphi_{s,v}$ determined in the section above, a sensitivity analysis was made to evaluate the effects of n_{CI} and n_T. From this, the values of n_{CI} and n_T for different fuel and oxygen carrier pairs can be determined, as seen in Fig. 11 using the EB ore and BP fuel pair as an example. Obviously, a constant gas conversion is calculated if the effect of oxygen carrier circulation is not considered, i.e. $n_{CI} = 0$, which is also the case for temperature, i.e. $n_T = 0$. Increase of either n_{CI} or n_T corresponds to increase the effect of solids circulation or temperature. Fig. 11(a) shows that the value of $n_{CI} = 3$ leads to a reasonably good fitting with the experimental results [22]. Keeping n_{CI} as 3, the use of different n_T is shown in Fig. 11(b), where $n_T = 18$ has the best fitting with experiments.

Similarly, the n_{CI} and n_T values were also determined for EB with SWC char and ilmenite with BP or SWC, see Table 6. Note that the n_T for ilmenite and SWC was not determined due to the lack of enough experimental data. In return, the values in Table 6 can reflect the performance of fuels, oxygen carrier and their interactions in the 10 kW$_{th}$ unit. The ξ indicates the char gasification efficiency, while $\varphi_{s,c}$ and $\varphi_{s,v}$ show the contact efficiency of the bed with gasification products and volatiles. Accordingly, the char gasification has an efficiency of $\xi = 0.98$ in the 10 kW$_{th}$ unit, which is higher than the 0.70 for a bituminous coal obtained in the 100 kW$_{th}$ unit used in a previous investigation [52]. This is expected since biomass fuels normally have better gasification reactivity than coal [86]. The contact efficiency of volatiles and bed in the 10 kW$_{th}$ unit has a slightly higher value of 0.20 than 0.15 found in the bigger 100 kW$_{th}$ unit [52], which is likely caused by the improvement from adding the volatiles distributor [10,87] in the 10 kW$_{th}$ system.

Table 5
Apparent rate constants (m^3/(kg·s)) for CH$_4$, CO and H$_2$ in the analytical model.

	$k_{F,CH4}$ [a]	$k_{F,CO}$ [b]	$k_{F,H2}$ [b]
EB	1.1·10^{-4}	6.6·10^{-3}	7.5·10^{-3}
Ilmenite	6.0·10^{-5}	3.0·10^{-3}	4.5·10^{-3}

[a] values for $\omega = 0.998$.
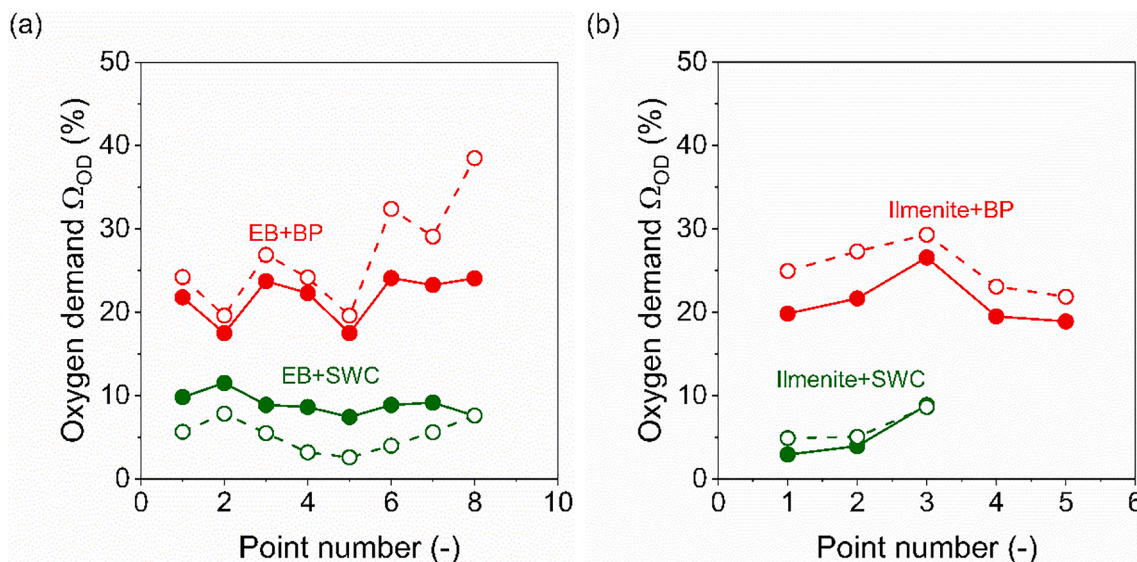[b] values for $\omega = 0.98$.

Fig. 10. Comparison of oxygen demand for modelling results (filled symbols) and experimental results (void symbols) from previous 10 kW$_{th}$ operation [22,59]: (a) "EB + BP" and "EB + SWC" pairs, (b) "Ilmenite + BP" and "Ilmenite + SWC" (only data at 1260 K) pairs.
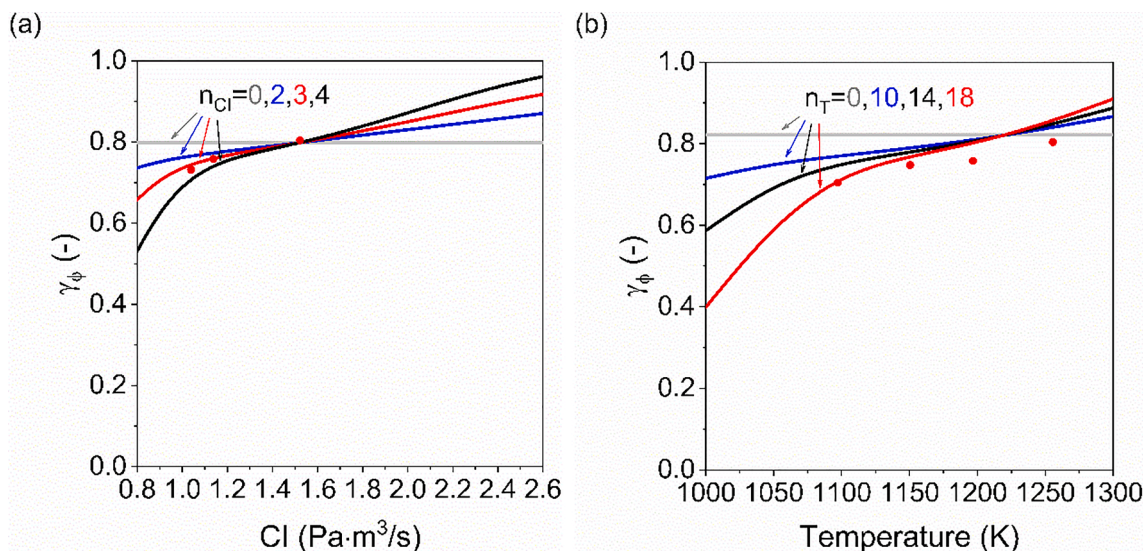

Fig. 11. Determination of (a) exponent n_{CI} for the effect of solids circulation and (b) exponent n_T for the effect of fuel reactor temperature by fitting the overall gas conversion with the experimental data from the previous 10 kW$_{th}$ operation [22].

Table 6
Values of various parameters determined and used in the analytical model.

	Fuel	ξ (-)	$\varphi_{s,c}$ (-)	$\varphi_{s,v}$ (-)	n_{CI} (-)	n_T (-)
EB	BP	0.98	0.90	0.20	3.0	18.0
EB	SWC	0.98	0.90	0.20	0.8	10.0
Ilmenite	BP	0.98	0.90	0.20	0.7	14
Ilmenite	SWC	0.98	0.90	0.20	4.0	–

6. Conclusions

In this work, reactivity data of a promising manganese ore oxygen carrier (EB) was determined in a batch fluidized-bed reactor and further used for analytical modelling as well as comparison from a 10 kW$_{th}$ pilot CLC reactor. It is confirmed that the EB ore has a low intensity of gas-phase oxygen release, with<0.5% O_2 detected in N_2 atmosphere at 1223 K, which motivates the use of a first order reaction rate constant. Reactions with CH_4 and syngas indicate that the EB ore has a better reactivity than ilmenite. The stable rate constants for EB are $1.1\cdot10^{-4}$ m^3/(kg·s) for CH_4 at the oxygen carrier conversion of 0.998, $6.6\cdot10^{-3}$ m^3/(kg·s) for CO and $7.5\cdot10^{-3}$ m^3/(kg·s) for H_2 at the oxygen carrier conversion of 0.98. Using these rate constants in the analytical reactor model, the overall gas conversion and oxygen demand were simulated, which fit well with the previous 10 kW$_{th}$ experiments. Accordingly, the biomass fuels had a high gasification fraction of 0.98 in the fuel reactor of the 10 kW$_{th}$ unit, while the contact efficiency of volatiles with bed material had a slightly higher value of 0.20 than previous results with gaseous and solid fuels in pilot operation.

Declaration of Competing Interest

The authors declare that they have no known competing financial interests or personal relationships that could have appeared to influence the work reported in this paper.

Acknowledgements

This work was carried out as part of the OxyCar-FBC project, which is conducted within the framework of ERA-NET Bioenergy and funded by the Swedish Energy Agency (P43936-1). Special thanks to Fredrik Hildor for the valuable suggestions on batch-reactor experiments.

References

[1] International Energy Agency. The role of CCUS in low-carbon power systems. Paris: IEA; 2020. https://www.iea.org/reports/the-role-of-ccus-in-low-carbon-power-systems.

[2] J. Adánez, A. Abad, T. Mendiara, P. Gayán, L.F. de Diego, F. García-Labiano, Chemical looping combustion of solid fuels, Prog. Energy Combust. Sci. 65 (2018) 6–66, https://doi.org/10.1016/j.pecs.2017.07.005.

[3] A. Lyngfelt, Chemical looping combustion: status and development challenges, Energy Fuels 34 (8) (2020) 9077–9093, https://doi.org/10.1021/acs.energyfuels.0c01454.

[4] M. Ishida, H. Jin, A new advanced power-generation system using chemical-looping combustion, Energy 19 (4) (1994) 415–422, https://doi.org/10.1016/0360-5442(94)90120-1.

[5] T. Mattisson, A. Lyngfelt, Capture of CO₂ using chemical-looping combustion, 1st Biennial Meeting of the Scandinavian-Nordic Section of the Combustion Institute, Gothenburg, Sweden, 2001.

[6] T. Mendiara, F. García-Labiano, A. Abad, P. Gayán, L.F. de Diego, M.T. Izquierdo, J. Adánez, Negative CO₂ emissions through the use of biofuels in chemical looping technology: A review, Appl. Energy 232 (2018) 657–684, https://doi.org/10.1016/j.apenergy.2018.09.201.

[7] J. Wolf, M. Anheden, J. Yan, Performance of Power Generation Processes with Chemical-Looping Combustion for CO Removals Requirements for the Oxidation and Reduction Reactors, International Pittsburgh Coal Conference, Newcastle, Australia, 2001.

[8] H. Jin, M. Ishida, Investigation of a novel gas turbine cycle with coal gas fueled chemical-looping combustion, American Society of Mechanical Engineers, Advanced Energy Systems Division (Publication) AES 40 (2000) 547–552.

[9] E. Jerndal, T. Mattisson, A. Lyngfelt, Thermal analysis of chemical-looping combustion, Chem. Eng. Res. Des. 84 (9) (2006) 795–806, https://doi.org/10.1205/cherd05020.

[10] A. Lyngfelt, B. Leckner, A 1000 MWth boiler for chemical-looping combustion of solid fuels – Discussion of design and costs, Appl. Energy 157 (2015) 475–487, https://doi.org/10.1016/j.apenergy.2015.04.057.

[11] C. Linderholm, P. Knutsson, M. Schmitz, P. Markström, A. Lyngfelt, Material balances of carbon, sulfur, nitrogen and ilmenite in a 100kW CLC reactor system, Int. J. Greenhouse Gas Control 27 (2014) 188–202, https://doi.org/10.1016/j.ijggc.2014.05.001.

[12] A. Abad, R. Pérez-Vega, L.F. de Diego, F. García-Labiano, P. Gayán, J. Adánez, Design and operation of a 50 kWth Chemical Looping Combustion (CLC) unit for solid fuels, Appl. Energy 157 (2015) 295–303, https://doi.org/10.1016/j.apenergy.2015.03.094.

[13] J. Ströhle, M. Orth, B. Epple, Chemical looping combustion of hard coal in a 1 MWth pilot plant using ilmenite as oxygen carrier, Appl. Energy 157 (2015) 288–294, https://doi.org/10.1016/j.apenergy.2015.06.035.

[14] H. Thunman, F. Lind, C. Breitholtz, N. Berguerand, M. Seemann, Using an oxygen-carrier as bed material for combustion of biomass in a 12-MWth circulating fluidized-bed boiler, Fuel 113 (2013) 300-309. https://doi.org /10.1016/j.fuel.2013.05.073.

[15] C. Linderholm, M. Schmitz, Chemical-looping combustion of solid fuels in a 100kW dual circulating fluidized bed system using iron ore as oxygen carrier, J. Environ. Chem. Eng. 4 (1) (2016) 1029–1039, https://doi.org/10.1016/j.jece:2016.01.006.

[16] T. Mendiara, L.F. de Diego, F. García-Labiano, P. Gayán, A. Abad, J. Adánez, On the use of a highly reactive iron ore in Chemical Looping Combustion of different coals, Fuel 126 (2014) 239–249, https://doi.org/10.1016/j.fuel.2014.02.061.

[17] T. Song, T. Shen, L. Shen, J. Xiao, H. Gu, S. Zhang, Evaluation of hematite oxygen carrier in chemical-looping combustion of coal, Fuel 104 (2013) 244–252, https://doi.org/10.1016/j.fuel.2012.09.030.

[18] J. Ma, H. Zhao, X. Tian, Y. Wei, S. Rajendran, Y. Zhang, S. Bhattacharya, C. Zheng, Chemical looping combustion of coal in a 5kWth interconnected fluidized bed reactor using hematite as oxygen carrier, Appl. Energy 157 (2015) 304–313, https://doi.org/10.1016/j.apenergy.2015.03.124.

[19] T. Pikkarainen, I. Hiltunen, Chemical looping combustion of solid biomass – performance of ilmenite and braunite as oxygen carrier materials, European Biomass Conference & Exhibition, Stockholm, Sweden, 2017.

[20] A. Abad, P. Gayán, T. Mendiara, J.A. Bueno, F. García-Labiano, L.F. de Diego, J. Adánez, Assessment of the improvement of chemical looping combustion of coal by using a manganese ore as oxygen carrier, Fuel Process. Technol. 176 (2018) 107–118, https://doi.org/10.1016/j.fuproc.2018.03.026.

[21] M. Schmitz, C. Linderholm, Chemical looping combustion of biomass in 10- and 100-kW pilots – Analysis of conversion and lifetime using a sintered manganese ore, Fuel 231 (2018) 73–84, https://doi.org/10.1016/j.fuel.2018.05.071.

[22] D. Mei, A.H. Soleimanisalim, C. Linderholm, A. Lyngfelt, T. Mattisson, Reactivity and lifetime assessment of an oxygen releasable manganese ore with biomass fuels in a 10 kWth pilot rig for chemical looping combustion, Fuel Process. Technol. 215 (2021) 106743, https://doi.org/10.1016/j.fuproc.2021.106743.

[23] D. Mei, T. Mendiara, A. Abad, L.F. de Diego, F. García-Labiano, P. Gayán, J. Adánez, H. Zhao, Manganese Minerals as Oxygen Carriers for Chemical Looping Combustion of Coal, Ind. Eng. Chem. Res. 55 (22) (2016) 6539–6546, https://doi.org/10.1021/acs.iecr.6b00263.

[24] P. Moldenhauer, A. Serrano, F. García-Labiano, L.F. de Diego, M. Biermann, T. Mattisson, A. Lyngfelt, Chemical-Looping Combustion of Kerosene and Gaseous Fuels with a Natural and a Manufactured Mn–Fe-Based Oxygen Carrier, Energy Fuels 32 (8) (2018) 8803–8816, https://doi.org/10.1021/acs.energyfuels.8b0158810.1021/acs.energyfuels.8b01588.s001.

[25] C. Linderholm, A. Lyngfelt, A. Cuadrat, E. Jerndal, Chemical-looping combustion of solid fuels – Operation in a 10 kW unit with two fuels, above-bed and in-bed fuel feed and two oxygen carriers, manganese ore and ilmenite, Fuel 102 (2012) 808–822, https://doi.org/10.1016/j.fuel.2012.05.010.

[26] C. Linderholm, A. Lyngfelt, C. Dueso, Chemical-looping combustion of solid fuels in a 10 kW reactor system using natural minerals as oxygen carrier, Energy Procedia 37 (2013) 598–607, https://doi.org/10.1016/j.egypro.2013.05.147.

[27] A. Abad, M. de las Obras-Loscertales, F. García-Labiano, L.F. de Diego, P. Gayán, J. Adánez, In situ gasification Chemical-Looping Combustion of coal using limestone as oxygen carrier precursor and sulphur sorbent, Chem. Eng. J. 310 (2017) 226–239, https://doi.org/10.1016/j.cej.2016.10.113.

[28] A. Levasseur, Alstom's Limestone-based Chemical Looping Development For Advanced Gasification, DOE Workshop: Gasification Systems and Coal & Biomass to Liquids, Morgantown, United States, 2015.

[29] M. Arjmand, H. Leion, T. Mattisson, A. Lyngfelt, Investigation of different manganese ores as oxygen carriers in chemical-looping combustion (CLC) for solid fuels, Appl. Energy 113 (2014) 1883–1894, https://doi.org/10.1016/j.apenergy.2013.06.015.

[30] D. Mei, T. Mendiara, A. Abad, L.F. de Diego, F. García-Labiano, P. Gayán, J. Adánez, H. Zhao, Evaluation of Manganese Minerals for Chemical Looping Combustion, Energy Fuels 29 (10) (2015) 6605–6615, https://doi.org/10.1021/acs.energyfuels.5b01293.

[31] A. Lyngfelt, B. Leckner, SO₂ capture fluidised-bed boilers: re-emission of SO₂ due to reduction of CaSO₄, Chem. Eng. Sci. 44 (2) (1989) 207–213, https://doi.org/10.1016/0009-2509(89)85058-4.

[32] L. Shen, M. Zheng, J. Xiao, R. Xiao, A mechanistic investigation of a calcium-based oxygen carrier for chemical looping combustion, Combust. Flame 154 (3) (2008) 489–506, https://doi.org/10.1016/j.combustflame.2008.04.017.

[33] T. Mattisson, A. Lyngfelt, H. Leion, Chemical-looping with oxygen uncoupling for combustion of solid fuels, Int. J. Greenhouse Gas Control 3 (1) (2009) 11–19, https://doi.org/10.1016/j.ijggc.2008.06.002.

[34] S. Sundqvist, T. Mattisson, H. Leion, A. Lyngfelt, Oxygen release from manganese ores relevant for chemical looping with oxygen uncoupling conditions, Fuel 232 (2018) 693–703, https://doi.org/10.1016/j.fuel.2018.06.024.

[35] P. Frohn, M. Arjmand, G. Azimi, H. Leion, T. Mattisson, A. Lyngfelt, On the high-gasification rate of Brazilian manganese ore in chemical-looping combustion (CLC) for solid fuels, AIChE J. 59 (11) (2013) 4346–4354, https://doi.org/10.1002/aic.v59.1110.1002/aic.14168.

[36] M. Keller, H. Leion, T. Mattisson, Mechanisms of Solid Fuel Conversion by Chemical-Looping Combustion (CLC) using Manganese Ore: Catalytic Gasification by Potassium Compounds, Energy Technol. 1 (4) (2013) 273–282, https://doi.org/10.1002/ente.v1.410.1002/ente.201200052.

[37] A. Pérez-Astray, T. Mendiara, L.F. de Diego, A. Abad, F. García-Labiano, M.T. Izquierdo, J. Adánez, Improving the oxygen demand in biomass CLC using manganese ores, Fuel 274 (2020) 117803, https://doi.org/10.1016/j.fuel.2020.117803.

[38] M. Rydén, A. Lyngfelt, T. Mattisson, Combined manganese/iron oxides as oxygen carrier for chemical looping combustion with oxygen uncoupling (CLOU) in a circulating fluidized bed reactor system, Energy Procedia 4 (2011) 341–348, https://doi.org/10.1016/j.egypro.2011.01.060.

[39] T. Berdugo, F. Lind, M. Rydén, H. Thunman, Experience of more than 1000 h of operation with oxygen carriers and solid biomass at large scale, Appl. Energy 190 (2017) 1174–1183, https://doi.org/10.1016/j.apenergy.2017.01.032.

[40] D. Mei, C. Linderholm, A. Lyngfelt, Performance of an oxy-polishing step in the 100 kWth chemical looping combustion prototype, Chem. Eng. J. 409 (2021) 128202, https://doi.org/10.1016/j.cej.2020.128202.

[41] N. Berguerand, A. Lyngfelt, Design and operation of a 10 kWth chemical-looping combustor for solid fuels – Testing with South African coal, Fuel 87 (12) (2008) 2713–2726, https://doi.org/10.1016/j.fuel.2008.03.008.

[42] P. Moldenhauer, S. Sundqvist, T. Mattisson, C. Linderholm, Chemical-looping combustion of synthetic biomass-volatiles with manganese-ore oxygen carriers, Int. J. Greenhouse Gas Control 71 (2018) 239–252, https://doi.org/10.1016/j.ijggc.2018.02.021.

[43] M. Schmitz, C. Linderholm, P. Hallberg, S. Sundqvist, A. Lyngfelt, Chemical-Looping Combustion of Solid Fuels Using Manganese Ores as Oxygen Carriers, Energy Fuels 30 (2016) 1204–1216, https://doi.org/10.1021/acs.energyfuels.5b02440.

[44] C. Linderholm, M. Schmitz, M. Biermann, M. Hanning, A. Lyngfelt, Chemical-looping combustion of solid fuel in a 100 kW unit using sintered manganese ore as oxygen carrier, Int. J. Greenhouse Gas Control 65 (2017) 170–181, https://doi.org/10.1016/j.ijggc.2017.07.017.

[45] L. Xu, H. Sun, Z. Li, N. Cai, Experimental study of copper modified manganese ores as oxygen carriers in a dual fluidized bed reactor, Appl. Energy 162 (2016) 940–947, https://doi.org/10.1016/j.apenergy.2015.10.167.

[46] L. Liu, Z. Li, L. Wang, Z. Zhao, Y.e. Li, N. Cai, MgO–Kaolin-Supported Manganese Ores as Oxygen Carriers for Chemical Looping Combustion, Ind. Eng. Chem. Res. 59 (15) (2020) 7238–7246, https://doi.org/10.1021/acs.iecr.9b05267.

[47] D. Mei, A. Abad, H. Zhao, S. Yan, B. Wang, Q. Yuan, Extension and evaluation of a macroscopic model for syngas-fueled chemical looping combustion, Chem. Eng. Process. - Process Intensification 133 (2018) 106–116, https://doi.org/10.1016/j.cep.2018.10.003.

[48] M. Su, H. Zhao, J. Ma, Computational fluid dynamics simulation for chemical looping combustion of coal in a dual circulation fluidized bed, Energy Convers. Manage. 105 (2015) 1–12, https://doi.org/10.1016/j.enconman.2015.07.042.

[49] P. Ohlemüller, F. Alobaid, A. Gunnarsson, J. Ströhle, B. Epple, Development of a process model for coal chemical looping combustion and validation against 100 kW$_{th}$ tests, Appl. Energy 157 (2015) 433–448, https://doi.org/10.1016/j.apenergy.2015.05.088.

[50] F. Alobaid, P. Ohlemüller, J. Ströhle, B. Epple, Extended Euler-Euler model for the simulation of a 1 MW$_{th}$ chemical–looping pilot plant, Energy 93 (2015) 2395–2405, https://doi.org/10.1016/j.energy.2015.10.107.

[51] A. Abad, P. Gayán, L.F. de Diego, F. García-Labiano, J. Adánez, Fuel reactor modelling in chemical-looping combustion of coal: 1. model formulation, Chem. Eng. Sci. 87 (2013) 277–293, https://doi.org/10.1016/j.ces.2012.10.006.

[52] P. Markström, C. Linderholm, A. Lyngfelt, Analytical model of gas conversion in a 100 kW chemical-looping combustor for solid fuels—Comparison with operational results, Chem. Eng. Sci. 96 (2013) 131–141, https://doi.org/10.1016/j.ces.2013.04.001.

[53] P. Kolbitsch, T. Pröll, H. Hofbauer, Modeling of a 120kW chemical looping combustion reactor system using a Ni-based oxygen carrier, Chem. Eng. Sci. 64 (1) (2009) 99–108, https://doi.org/10.1016/j.ces.2008.09.014.

[54] S. Banerjee, Full-Loop Simulation of the Combustion of Biomass in a Circulating Fluidized Bed Combustor; DOE/NETL-2021/2650; NETL Technical Report Series; U.S. Department of Energy, National Energy Technology Laboratory: Morgantown, WV, 2021; p 52. https://doi.org/10.2172/1785675.

[55] S. Banerjee, R.K. Agarwal, An Eulerian Approach to Computational Fluid Dynamics Simulation of a Chemical-Looping Combustion Reactor With Chemical Reactions, J. Energy Resour. Technol. 138 (2016), 042201, https://doi.org/10.1115/1.4031968.

[56] A. Abad, J. Adánez, P. Gayán, L.F. de Diego, F. García-Labiano, G. Sprachmann, Conceptual design of a 100 MW$_{th}$ CLC unit for solid fuel combustion, Appl. Energy 157 (2015) 462–474, https://doi.org/10.1016/j.apenergy.2015.04.043.

[57] A. Abad, P. Gayán, F. García-Labiano, L.F. de Diego, J. Adánez, Relevance of oxygen carrier characteristics on CLC design for gaseous fuels, 3rd International Conference on Chemical Looping, Gothenburg, Sweden, 2014.

[58] N. Berguerand, A. Lyngfelt, T. Mattisson, P. Markström, Chemical Looping Combustion of Solid Fuels in a 10 kW$_{th}$ Unit, Oil Gas Sci, Technol. – Rev. IFP Energies nouvelles 66 (2) (2011) 181–191, https://doi.org/10.2516/ogst/2010023.

[59] I. Gogolev, A.H. Soleimanisalim, C. Linderholm, A. Lyngfelt, Commissioning, performance benchmarking, and investigation of alkali emissions in a 10 kW$_{th}$ solid fuel chemical looping combustion pilot, Fuel 287 (2021), 119530, https://doi.org/10.1016/j.fuel.2020.119530.

[60] J. Adánez, A. Cuadrat, A. Abad, P. Gayán, L.F. de Diego, F. García-Labiano, Ilmenite Activation during Consecutive Redox Cycles in Chemical-Looping Combustion, Energy Fuels 24 (2) (2010) 1402–1413, https://doi.org/10.1021/ef900856d.

[61] H. Leion, A. Lyngfelt, M. Johansson, E. Jerndal, T. Mattisson, The use of ilmenite as an oxygen carrier in chemical-looping combustion, Chem. Eng. Res. Des. 86 (9) (2008) 1017–1026, https://doi.org/10.1016/j.cherd.2008.03.019.

[62] A. Cuadrat, A. Abad, F. García-Labiano, P. Gayán, L.F. de Diego, J. Adánez, The use of ilmenite as oxygen-carrier in a 500W$_{th}$ Chemical-Looping Coal Combustion unit, Int. J. Greenhouse Gas Control 5 (6) (2011) 1630–1642, https://doi.org/10.1016/j.ijggc.2011.09.010.

[63] Z. Huang, N.a. Gao, Y. Lin, G. Wei, K. Zhao, A. Zheng, Z. Zhao, H. Yuan, H. Li, Exploring the migration and transformation of lattice oxygen during chemical looping with NiFe$_2$O$_4$ oxygen carrier, Chem. Eng. J. 429 (2022) 132064, https://doi.org/10.1016/j.cej.2021.132064.

[64] F. Hildor, H. Leion, C.J. Linderholm, T. Mattisson, Steel converter slag as an oxygen carrier for chemical-looping gasification, Fuel Process Technol. 210 (2020) 106576, https://doi.org/10.1016/j.fuproc.2020.106576.

[65] H. Leion, T. Mattisson, A. Lyngfelt, Use of Ores and Industrial Products As Oxygen Carriers in Chemical-Looping Combustion, Energy Fuels 23 (2009) 2307–2315, https://doi.org/10.1021/ef8008629.

[66] H. Leion, V. Frick, F. Hildor, Experimental Method and Setup for Laboratory Fluidized Bed Reactor Testing, Energies 11 (2018) 2505, https://doi.org/10.3390/en11102505.

[67] P. Cho, T. Mattisson, A. Lyngfelt, Defluidization conditions for a fluidized bed of iron oxide-, nickel oxide-, and manganese oxide-containing oxygen carriers for chemical-looping combustion, Ind. Eng. Chem. Res. 45 (3) (2006) 968–977, https://doi.org/10.1021/ie050484d.

[68] V. Purnomo, D. Yilmaz, H. Leion, T. Mattisson, Study of defluidization of iron- and manganese-based oxygen carriers under highly reducing conditions in a lab-scale fluidized-bed batch reactor, Fuel Process Technol. 219 (2021) 106874, https://doi.org/10.1016/j.fuproc.2021.106874.

[69] G.L. Schwebel, H. Leion, W. Krumm, Comparison of natural ilmenites as oxygen carriers in chemical-looping combustion and influence of water gas shift reaction on gas composition, Chem. Eng. Res. Des. 90 (9) (2012) 1351–1360, https://doi.org/10.1016/j.cherd.2011.11.017.

[70] S. Sundqvist, M. Arjmand, T. Mattisson, M. Rydén, A. Lyngfelt, Screening of different manganese ores for chemical-looping combustion (CLC) and chemical-looping with oxygen uncoupling (CLOU), Int. J. Greenhouse Gas Control 43 (2015) 179–188, https://doi.org/10.1016/j.ijggc.2015.10.027.

[71] G.A. Matthesius, R.M. Morris, M.J. Desai, Prediction of the volatile matter in coal from ultimate and proximate anayses, J. S. Afr. Inst. Min. Metall. 87 (1987) 157–161.

[72] A. Abad, A. Cuadrat, T. Mendiara, F. García-Labiano, P. Gayán, J. Adánez, Low-Cost Fe-Based Oxygen Carrier Materials for the iG-CLC Process with Coal. 2, Ind. Eng. Chem. Res. 51 (50) (2012) 16230–16241, https://doi.org/10.1021/ie302158q.

[73] N. Berguerand, A. Lyngfelt, Design and operation of a 10kW$_{th}$ chemical-looping combustor for solid fuels – Testing with South African coal, Fuel 87 (12) (2008) 2713–2726, https://doi.org/10.1016/j.fuel.2008.03.008.

[74] T. Mattisson, A. Lyngfelt, P. Cho, The use of iron oxide as an oxygen carrier in chemical-looping combustion of methane with inherent separation of CO$_2$, Fuel 80 (13) (2001) 1953–1962, https://doi.org/10.1016/S0016-2361(01)00051-5.

[75] M.M. Azis, E. Jerndal, H. Leion, T. Mattisson, A. Lyngfelt, On the evaluation of synthetic and natural ilmenite using syngas as fuel in chemical-looping combustion (CLC), Chem. Eng. Res. Des. 88 (11) (2010) 1505–1514, https://doi.org/10.1016/j.cherd.2010.03.006.

[76] T. Mattisson, E. Jerndal, C. Linderholm, A. Lyngfelt, Reactivity of a spray-dried NiO/NiAl$_2$O$_4$ oxygen carrier for chemical-looping combustion, Chem. Eng. Sci. 66 (20) (2011) 4636–4644, https://doi.org/10.1016/j.ces.2011.06.025.

[77] D. Jing, M. Jacobs, P. Hallberg, A. Lyngfelt, T. Mattisson, Development of CaMn$_{0.775}$Mg$_{0.125}$Ti$_{0.125}$O$_{3-\delta}$ oxygen carriers produced from different Mn and Ti sources, Mater. Des. 89 (2016) 527–542, https://doi.org/10.1016/j.matdes.2015.09.117.

[78] S. Sundqvist, N. Khalilian, H. Leion, T. Mattisson, A. Lyngfelt, Manganese ores as oxygen carriers for chemical-looping combustion (CLC) and chemical-looping with oxygen uncoupling (CLOU), J. Environ. Chem. Eng. 5 (3) (2017) 2552–2563, https://doi.org/10.1016/j.jece:2017.05.007.

[79] P. Gayán, I. Adánez-Rubio, A. Abad, L.F. de Diego, F. García-Labiano, J. Adánez, Development of Cu-based oxygen carriers for Chemical-Looping with Oxygen Uncoupling (CLOU) process, Fuel 96 (2012) 226–238, https://doi.org/10.1016/j.fuel.2012.01.021.

[80] D. Mei, H. Zhao, Z. Ma, C. Zheng, Using the Sol–Gel-Derived CuO/CuAl$_2$O$_4$ Oxygen Carrier in Chemical Looping with Oxygen Uncoupling for Three Typical Coals, Energy Fuels 27 (5) (2013) 2723–2731, https://doi.org/10.1021/ef3021602.

[81] I. Adánez-Rubio, A. Abad, P. Gayán, L.F. de Diego, F. García-Labiano, J. Adánez, Identification of operational regions in the Chemical-Looping with Oxygen Uncoupling (CLOU) process with a Cu-based oxygen carrier, Fuel 102 (2012) 634–645, https://doi.org/10.1016/j.fuel.2012.06.063.

[82] A. Abad, I. Adánez-Rubio, P. Gayán, F. García-Labiano, L.F. de Diego, J. Adánez, Demonstration of chemical-looping with oxygen uncoupling (CLOU) process in a 1.5 kW$_{th}$ continuously operating unit using a Cu-based oxygen-carrier, Int. J. Greenhouse Gas Control 6 6 (2012) 189–200, https://doi.org/10.1016/j.ijggc.2011.10.016.

[83] O. Levenspiel, Chemical reaction engineering, Wiley, New York, 1972.

[84] A. Abad, J. Adánez, F. García-Labiano, L.F. de Diego, P. Gayán, J. Celaya, Mapping of the range of operational conditions for Cu-, Fe-, and Ni-based oxygen carriers in chemical-looping combustion, Chem. Eng. Sci. 62 (1-2) (2007) 533–549, https://doi.org/10.1016/j.ces.2006.09.019.

[85] N. Berguerand, Design and Operation of a 10 kW$_{th}$ Chemical-Looping Combustor for Solid Fuels, PhD Thesis, Chalmers University of Technology, Gothenburg, Sweden, 2009.

[86] A. Abad, T. Mendiara, L.F. de Diego, F. García-Labiano, P. Gayán, J. Adánez, A simple model for comparative evaluation of different oxygen carriers and solid fuels in iG-CLC processes, Fuel Process Technol. 179 (2018) 444–454, https://doi.org/10.1016/j.fuproc.2018.07.031.

[87] X. Li, A. Lyngfelt, T. Mattisson, An experimental study of a volatiles distributor for solid fuels chemical-looping combustion process, Fuel Process Technol. 220 (2021) 106898, https://doi.org/10.1016/j.fuproc.2021.106898.